Nov 9th, 12:00 AM - 12:00 AM

Finite Element Investigations of the Effect of Residual Stress in Cold-Formed Sigma Beams

Feiliang Wang

Jian Yang

Wei-Wen Yu International Specialty Conference on Cold-Formed Steel Structures
Baltimore, Maryland, U.S.A, November 9 & 10, 2016

Finite element investigations of the effect of residual stress in cold-formed sigma beams

Feiliang Wang[1], Jian Yang[2]

Abstract

Press braking is a cold forming operation used to fold the angle along the flat sheet between the top punch and bottom die. The residual stress will be induced in this process as a result of plastic deformation. In the welding process, a dynamic thermal cycle is introduced to generate a non-uniformly temperature distribution on the heat affected zone (HAZ), and the residual stress also occurs in the process as a result of uneven cooling along the welding bead. The existence of residual stress can superimpose onto the external loadings to affect the stiffness and load resistance capacity of the structures. Therefore, a comprehensive understanding of the distribution and the impact of residual stress on the performance of cold-formed sections (CFS) is essential.

The primary motivation of this paper is to provide a numerical solution for exploring the effect of press braking and welding residual stress on CFS sigma beams. Modelling methods were validated against the published experimental data and the influence of inputs to the model was discussed by parametrical studies. Based on the laboratory test results, the effect of residual stress on sigma beams was further investigated. It is found that the residual stress on the corner region will increase the failure load of sigma beams while the residual stress on the flat portion will decrease the failure load.

Key words: Press braking; Welding process; Residual stress; Numerical solution; Laboratory test.

[1] *Post-doc at School of Naval Architecture, Ocean and Civil Engineering, Shanghai Jiaotong University, Shanghai, China (wongfayeleung@sjtu.edu.cn).*

[2] *Professor at School of Naval Architecture, Ocean and Civil Engineering, Shanghai Jiaotong University, Shanghai, China.*

1 Introduction

Residual stress is one of the main sources of material imperfections. As a manually manufacturing process, press braking is suitable for forming simple configurations such as angle and channel sections. The press braking induced residual stress can be achieved by analytical study **[1-3]**, laboratory test **[4]** and numerical simulation **[5]**. Welding is a coupled thermal-mechanical process which involves short-term localized heating and metallurgical transformation. The welding residual stress is still not well understood as the stress distribution is of a time-dependent nature and thus the theoretical and experimental prediction of welding residual stress can be rather challenging. However, the numerical simulation was considered as an efficient tool in the area thanks to the "birth and death" technique **[6-8]**. The technique can deactivate and reactive the elements by multiplying their stiffness by a reduction factor for simulating the movement of the heat source. The extensive studies demonstrated that the experimental efforts in welding residual stress can be reduced by adequate application of FE technique **[9, 10]**.

The presence of residual stress in a metal component can either be beneficial or detrimental to its load resistance capacity, depending on the magnitude and distribution of the stress. The effects of residual stress were veiled till the scholars from Lehigh University conducted a series of theoretical and experimental studies **[11-13]**. Then, **[14]** proposed a "second reduction method" to quantify the effect of residual stresses on the local buckling behaviour of a cold-formed section. More recently, numerical methods were widely introduced to study the influence of residual stress. **[15]** presented an advanced numerical approach for predicting the effect of cold work on press-braked thin walled steel columns and both residual stresses and the equivalent plastic strains were considered in the FE model. In the same year, **[16]** conducted a parametric study to explore the combined influence of isotropic hardening and kinematic hardening with residual stresses on the load-deformation responses of steel columns.

2 Numerical studies of press braking and welding process

2.1 Residual stress in channel section

In the modelling process, the press braking was simplified as a pure bending operation, as shown in Fig. 1. The sheet was placed between a set of top punch and bottom die and the angle was then achieved along the sheet when the punch moves downward to meet the shape of the die. For verifying the FEM, the

numerical result was compared with the test data of specimen P16 (see Fig. 2) presented in **[18]**. In the test, the specimen was saw-cut from the column with press-braked channel sections and the yield strength was 219MPa.

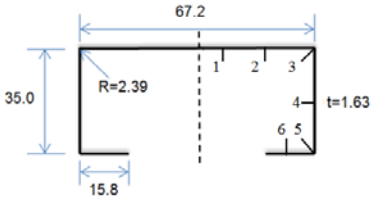

Figure 1: Press braking model **Figure 2: Geometric dimensions of P16**

An explicit analysis was conducted in the model for simulating the dynamic operation and shell element S4R and rigid element R3D4 were applied for the sheet and die, respectively. The hard contact was adopted as the normal interaction between tools and sheet to control the overclosure. There was no friction applied in the tangential direction on the interacted surfaces as it may cause extra surface stresses and strains. The meshed model and the stress contour are shown in the Figs. 3 and 4.

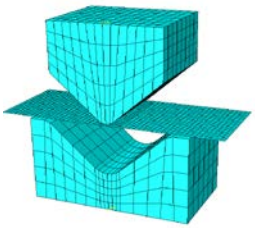

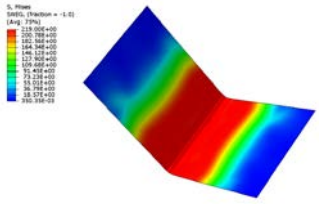

Figure 3: Mesh pattern **Figure 4: Von mises Stress contour**

The comparison of normalized strain in the longitudinal direction between experimental and numerical results is demonstrated in Fig. 5. The sign convention of the FEM model was positive for tension and negative for compression.

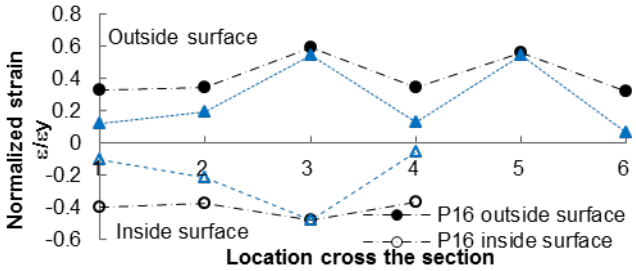

Figure 5: Comparison of the longitudinal strain

Fig. 5 shows a good agreement on the corner portion between FEM and test results, with the gaps at corner point 3 and 5 are 8.5% and 3.6%, respectively. The FEM achieved longitudinal strain is lower than laboratory measurement at flat portion because the effect of coiling-uncoiling was ignored in the model.

2.2 Residual stress in sigma sections

The same modelling method was further used for simulating the press braking of sigma section. The geometric dimensions of sigma sections are illustrated in Table 1.

Table 1: List of sigma sections

Section	Depth mm	Flange mm	Lip mm	Outer Web mm	Thickness mm	Corner radius mm
20012	200	62.5	20	45	1.2	4
20014	200	62.5	20	45	1.4	4
20024	200	62.5	20	45	2.4	4
24014	240	62.5	20	50	1.4	4
24024	240	62.5	20	50	2.4	4
30020	300	75	20	60	1.8	4
30030	300	75	20	60	3.0	4

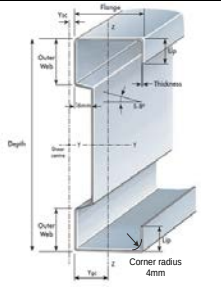

The distribution of longitudinal and transverse residual stresses along thickness on the corner portion is presented in Fig. 6.

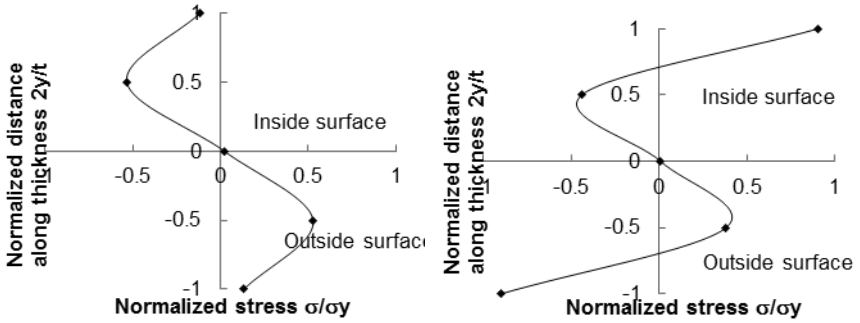

(a) In longitudinal direction (b) In transverse direction

Figure 6: Residual stress along thickness on the corner portion

It can be seen from the figure that the residual stress in both directions is non-linear along the shell thickness and asymmetric to the neutral axis. For the corner portion, the maximum longitudinal residual stress is $0.6\sigma_y$ locates on the quarter of thickness, while the peak transverse residual stress is $0.9\sigma_y$ on the

surface. A series of parametric studies were further conducted to investigate the sensibility of the stress result to the inputs. The press braking residual stress with yield strength 235MPa, 345MPa and 450MPa were compared in Fig. 7. Fig. 8 shows the comparison of press braking residual stress with different sheet thicknesses.

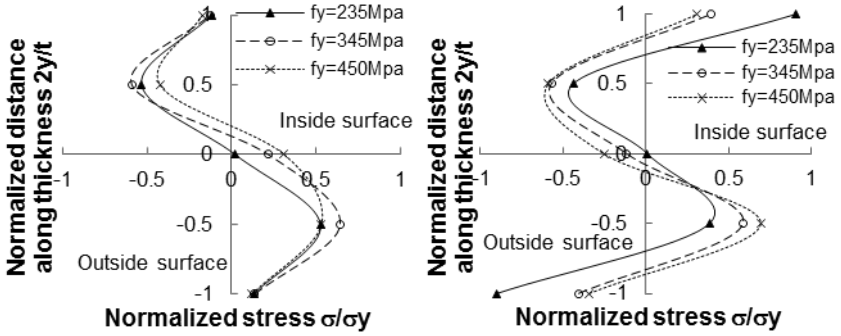

(a) Longitudinal residual stress (b) Transverse residual stress

Figure 7: Residual stress with different yield strengths on the corner

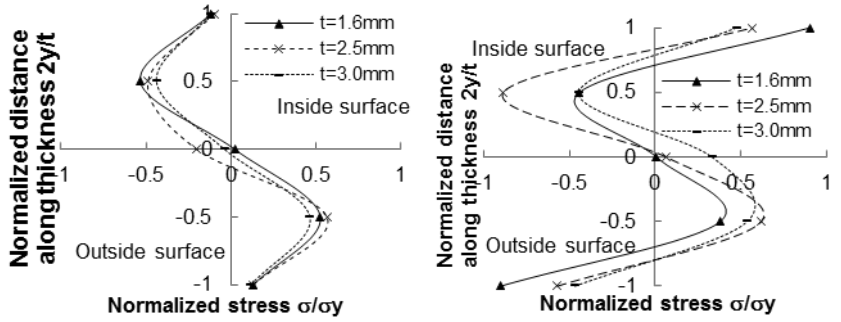

(a) Longitudinal residual stress (b) Transverse residual stress

Figure 8: Residual stress with different thicknesses on the corner

According to Fig. 7, the transverse residual stress on the corner reduces 56% and 25% with increasing yield strength from 235MPa, 345MPa to 450MPa. The effect of thickness on longitudinal residual stress on the corner portion is insignificant, as shown in Fig. 8, while the transverse residual stress decreases as the increase of shell thickness.

2.3 Modelling of welding process

In the thermal analysis, the specimen used in the model was a butt-welded sigma beam 20012, as shown in Fig. 9. It was assumed that the width of HAZ was

60mm on both sides of the weld bead and the effect of solid phase transformation and multi-pass welding was insignificant for thin walled section. A reference point and a reference path located on the middle of the HAZ were selected to characterise the distribution of temperature and residual stress (see Fig. 10). In the simulation, it was assumed that the temperature of parent metal was equal to ambient temperature (20℃) before welding, the entire heating time was 100s and the total cooling time was about 900s. The finite element formulation was based on the governing equation for transient nonlinear heat transfer (Eq. 1).

$$\frac{\partial}{\partial x}\left(k_x\frac{\partial T}{\partial x}\right)+\frac{\partial}{\partial y}\left(k_y\frac{\partial T}{\partial y}\right)+\frac{\partial}{\partial z}\left(k_z\frac{\partial T}{\partial z}\right)+Q=\rho C\frac{\partial T}{\partial t} \qquad \textbf{(Eq. 1)}$$

where k_x, k_y and k_z are the thermal conductivities in the x, y and z directions, respectively; T is the current temperature; Q is the heat generation; ρ is the density; C is the specific heat; and t is the time.

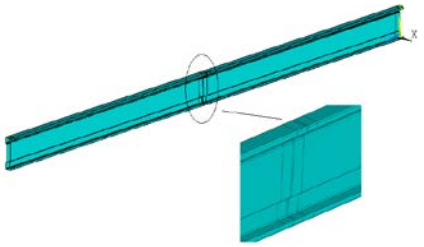

Figure 9: Overall view of the model

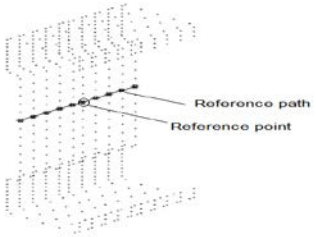

Figure 10: Reference point & path

As the material property is critical to the metallurgical conditions of the weldment and the results of thermal–mechanical analysis, the temperature-dependent material properties listed in Fig. 11 were used in the model.

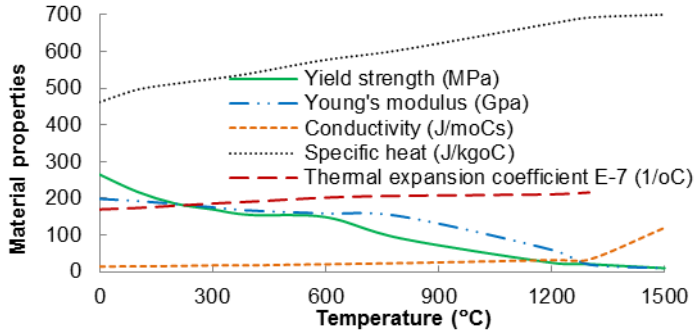

Figure 11: Temperature-dependent material properties (ref. to [20])

The Linear welding energy based on Eq.2 was applied in the model.

$$Q = \eta \frac{UI}{V} \quad \textbf{(Eq. 2)}$$

where Q is the net line energy; η is the arc efficiency; V is the travel speed; U and I are the arc voltage and current. In the analysis, the current was 140A, voltage was 9.5V, heat torch was travelling at a speed of 80 mm/min, and η was 0.5 for thin-walled sections **[21]**.

2.4 Result discussions

The visualized temperature flow at 20s, 50s, 100s and 1000s, respectively, is demonstrated in Fig. 12.

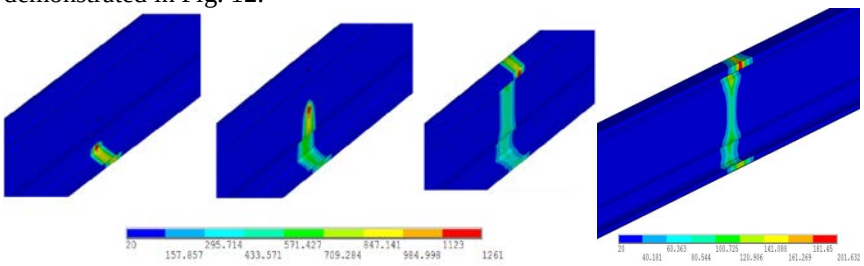

a) 20s b) 50s c) 100s d) 1000s

Figure 12: Temperature contours during welding process

It can be seen that the weldment is heated localized by the heat flux and temperature in the vicinity of the weld bead are non-uniformly distributed. The maximum temperature during welding is 1261℃ and then drop to 202℃ after cooling down. The numerical and experimental **[20]** obtained temperature history curves are illustrated in Figs. 13 and 14.

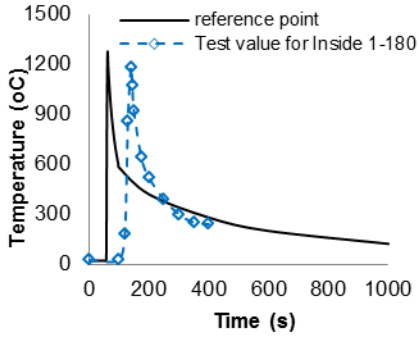

Figure 13: Temperature history

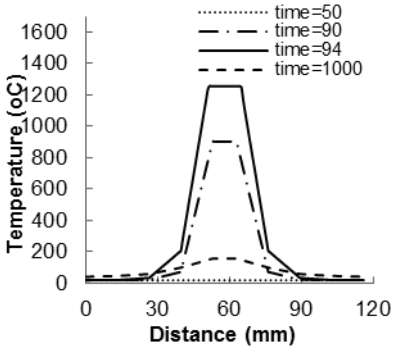

Figure 14: Temperature development

Fig. 13 shows that the peak temperature during the welding process is 1261℃ at reference point and decreases to 280℃ at 400s due to convection. The temperature history of the reference point shows a good agreement when compared to the test curve, while the experimental curve increases to peak temperature around 1190℃ at 140s and then reduces to 240℃ at 400s. It can be seen from Fig. 14 that the range of HAZ caused by torch is 60mm in width and for areas far from the weld bead, the value of the temperature is reduced to zero.

Mechanical analysis was conducted based on the achieved thermal field. It is assumed that the direction normal to the weld bead is the transverse direction and the direction of the weld bead is the longitudinal direction. Fig. 15 exhibits the distribution of longitudinal and transverse residual stress along the reference path after cooling down.

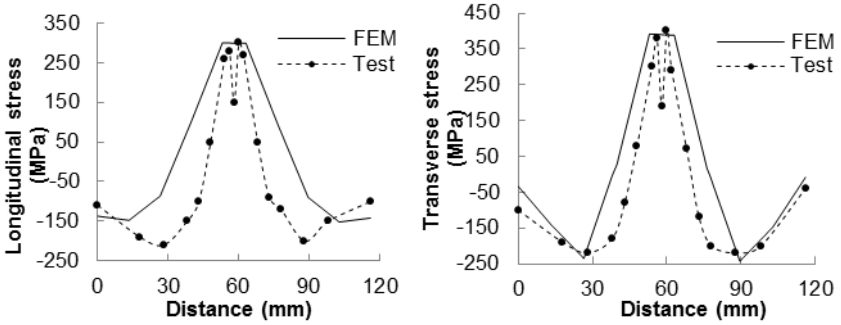

(a) Longitudinal residual stress (b) Transverse residual stress

Figure 15: Residual stress along reference path after cooling down

Fig. 15 shows that the maximum longitudinal stress is in tension and the max value is 300MPa. The transverse stress approaches to zero value almost 25mm away from the welding centreline; then tensile stress reverses to compressive residual stress.

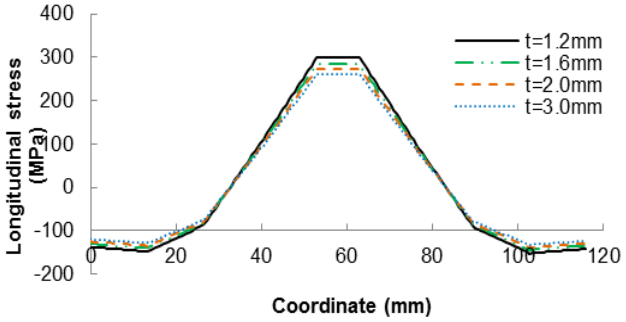

Figure 16: Longitudinal residual stress along the path

Fig. 16 shows that the maximum tensile stress and compressive stress decrease with the increases in shell thickness. The occurrence of this phenomenon because the increases in thickness will benefit to the convection process and thus lead to a lower temperature field and residual stress.

3 Simply supported beams with the influence of residual stress

The influence of welding and press braking process on the behaviour of simply supported single-span sigma beams was studied numerically herein. In the model, the preceding achieved distribution of press braking and welding residual stress was imported into FE program as initial stress. The numerical results were further validated by values obtained from laboratory test and analytical method.

3.1 Purlin-sheeting bending test under UDL

In the test, a vacuum box was introduced to simulate the uniformly distributed load (UDL) downward loading condition. A pair of simply-supported identical sigma purlins with 6m length was placed in parallel with opposing faces. The purlins were bolted by four steel angle cleats placed on two steel stands at both ends. The test setup is shown in Fig. 17. Each specimen was butt-welded together by three short press-braked components. The location of the weld bead is shown in Fig. 18. The cross-sectional geometric dimensions of each specimen can refer to the Table 1.

Figure 17: Overall test assemblies

Figure 18: The purlin with weld beads

3.2 Strain hardening

A series of tensile tests were conducted to obtain the stress-strain curve for each specimen. The strength enhancement during the press braking process was considered according to **[22, 23]**. The average yield strength f_{ya} of a cross section due to cold working was determined by Eq. 3 and the modified equation for plotting a enhanced stress-strain curve was based on Eqs. 4 and 5:

$$f_{ya} = f_{yb} + \left(f_u - f_{yb}\right)\frac{knt^2}{A_g} \quad \textbf{and} \quad f_{ya} \le \frac{f_u + f_{yb}}{2} \qquad \textbf{(Eq. 3)}$$

where A_g is the gross cross-sectional area; f_{yb} is the basic yield strength; k is a numerical coefficient that depends on the type of forming; n is the number of 90° bends in the cross section.

$$\begin{cases} \sigma = E\varepsilon & (\varepsilon \leq \frac{Y}{E}) \quad \textbf{(Eq. 4)} \\ \sigma = Y\left(\frac{E\varepsilon}{Y}\right)^n & (\varepsilon > \frac{Y}{E}) \quad \textbf{(Eq. 5)} \end{cases}$$

Where σ and ε are engineering stress and strain, respectively; E_0 is the material's Young's modulus; $\sigma_{0.2}$ is the material's 0.2% proof stress; n is a strain hardening exponent; Y is the yield strength. The tested and enhanced strength is summarised in Table 2.

Table 2: Summary of the test results

Specimen	Associated section thickness (mm)	Elastic modulus (GPa)	0.2% Proof strength (MPa)	Ultimate tensile strength (MPa)	Enhanced yield strength (MPa)
60-20012	1.2	203	178	344	206
60-20014	1.4	207	185	350	219
60-20024	2.4	213	201	352	255
60-24014	1.4	207	185	350	214
60-24024	2.4	213	201	352	252
60-30020	2.0	201	175	347	210
60-30030	3.0	206	186	324	233

3.3 Numerical modelling

In the simulations, the true material strength was adopted for the virgin model, and the enhanced strength was used for the models with the strain hardening effect. In the model, the vertical bolt supports were applied on the upper quarter of the circular arc of four bolt holes and lateral restraints were applied to all bolt holes as the bolt to beam interaction. The outerweb to flange junction line was fully restrained in lateral direction, represented the restraint of roof sheeting to the purlin. The UDL was applied along the middle of top-flange as the compression from sheeting (see Fig. 19).

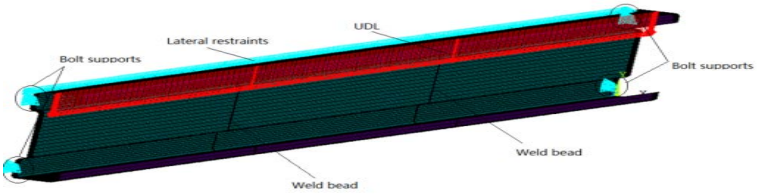

Figure 19: Model of simply supported sigma beam

Both press braking and welding residual stresses were considered as the initial stress. The welding residual stress was only applied to the HAZ and the distribution of welding and press braking residual stress in the longitudinal direction is shown in Fig. 20.

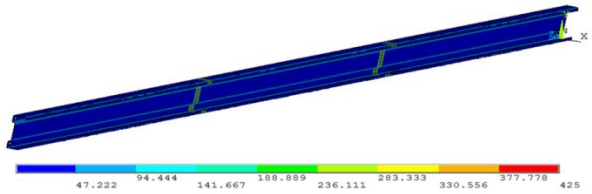

Figure 20: Combined residual stress

The experimental, numerical and theoretical load to deflection curves are shown in the Fig. 21. The model with only welding residual stress (only W) and the model with combined press braking residual stress and welding residual stress (PB and W) are all presented in the figure.

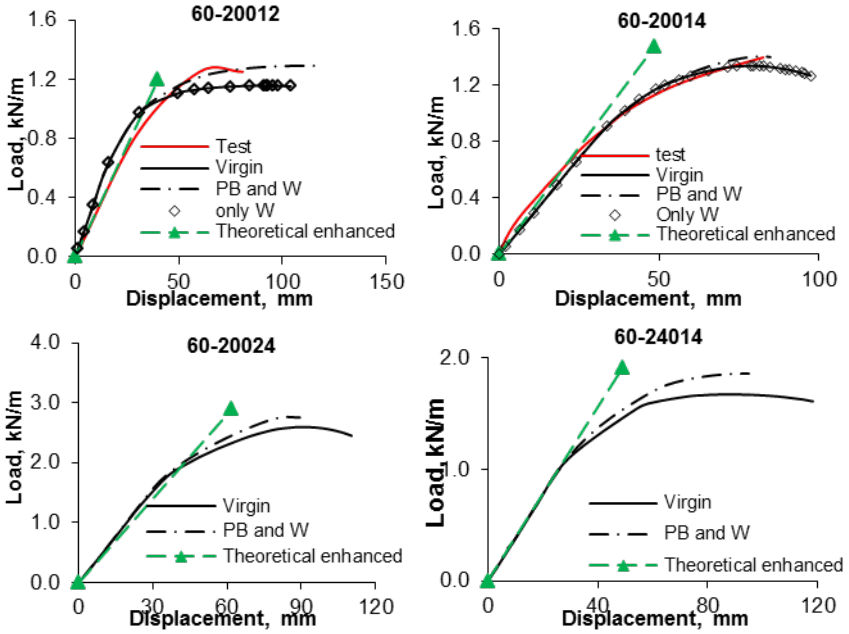

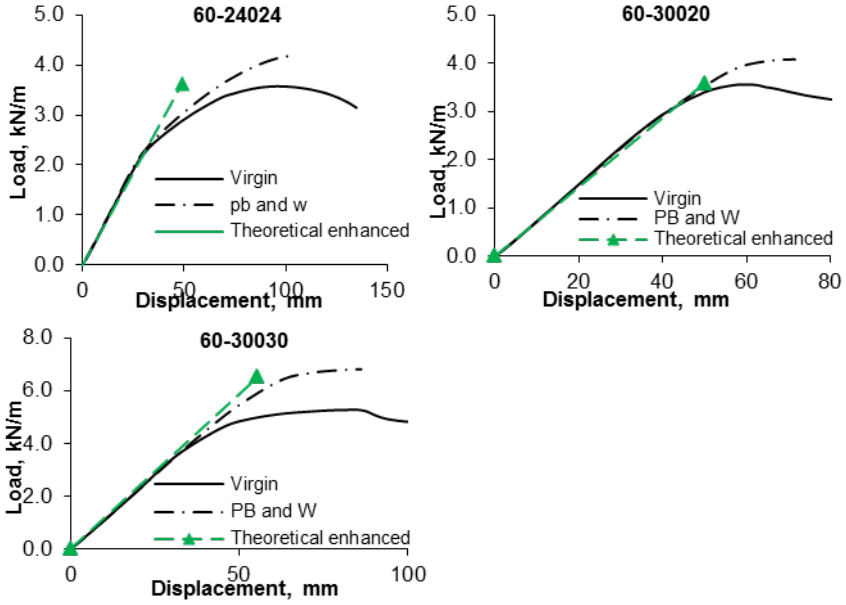

Figure 21: Load to deflection curves

By comparing the curves of virgin model and model with welding residual stress of specimen 60-20012 and 60-20014, it can be concluded that the effect of welding residual stress is insignificant on the load resistance capacity of sigma beam. Meanwhile, the load-deflection curves for all the specimens are enhanced by the effect of strain hardening during press braking. A good agreement can be found on the failure load of specimens between the theoretical curves and numerical curves. The theoretical curves show a greater stiffness than numerical curves when exceeding the yield stress due to the ignore of residual stress in the theoretical analysis.

In order to further investigate the effects of cold work, the failure loads of theoretical model with virgin material ($q_{T,v}$), theoretical model with press braking effect ($q_{T,pb}$), FE model with virgin material ($q_{FE,v}$) and FE model with effect of press braking and welding ($q_{FE,pb,w}$) are summarized in Table 3.

Table 3: List of failure loads

Specimens	Failure load (kN/m)				$q_{T,v}/q_{FE,v}$	$q_{T,pb}/q_{FE,pb,w}$	$q_{FE,pb,w}/q_{FE,}$
	$q_{T,v}$	$q_{T,pb}$	$q_{FE,v}$	$q_{FE,pb}$			
60-20012	1.05	1.20	1.16	1.29	0.91	0.93	1.11

60-20014	1.11	1.48	1.34	1.41	0.83	1.05	1.05
60-20024	2.45	2.89	2.59	2.76	0.95	1.05	1.07
60-24014	1.69	1.90	1.68	1.79	1.00	1.06	1.07
60-24024	3.15	3.63	3.57	4.18	0.88	0.87	1.17
60-30020	3.39	3.58	3.56	4.08	0.95	0.88	1.15
60-30030	5.40	6.51	5.28	6.81	1.02	0.96	1.29
Mean					**0.93**	**0.97**	**1.13**
S.D.					**0.07**	**0.08**	**0.08**

It can be found in Table 3 that the ratio between theoretical and FEM values with virgin model is 0.93, and the ratio between theoretical and FEM values with press braking and welding effect is 0.97, which indicates the reliability of the numerical approach. The enhancement of press braking process on failure load is achieved by comparing the FE enhanced model ($q_{FE,pb,w}$) with the virgin model ($q_{FE,v}$), and the average ratio is 1.13 with the maximum ratio is 1.29.

For exploring the effect of residual stress, more sensitivity studies are conducted by FEM. In the study, the effect of strain hardening is ignored and the virgin model is compared with two different models: the model with residual stress on both corner portion and flat portion (C+F) and the model only with corner residual stress (C). The failure loads for each model are listed in Table 4.

Table 4: List of failure loads

Specimens	**Failure load (kN/m)**			q_{C+F}/q_V	q_C/q_V
	q_V	q_{C+F}	q_C		
60-20012	1.16	1.10	1.17	0.95	1.01
60-20014	1.34	1.30	1.36	0.97	1.01
60-20024	2.59	2.51	2.62	0.97	1.01
60-24014	1.68	1.62	1.73	0.96	1.03
60-24024	3.57	3.51	3.59	0.98	1.01
60-30020	3.56	3.47	3.73	0.97	1.05
60-30030	5.28	5.22	5.52	0.99	1.05
Mean				**0.97**	**1.02**
S.D.				**0.01**	**0.02**

It can be found that the cold work in corner regions can enhance the load resistance of sigma beam, as the average enhancement of the failure load is 1.02.

While the residual stress in flat portions lead to reduce the failure load of each specimen. The average ratio of the failure load between the model with combined residual stress and virgin model is 0.97. The conclusion can be drawn that the effect of strain hardening is dominant for the enhancement of load resistance capacity of sigma beam with simply supported. The residual stress on the corner portion can increase the failure load while the cross-sectional residual stress will decrease the failure load.

4 Conclusions

The numerical results and discussions presented in the paper allow the following conclusions to be made:

1. The effect of yield strength on residual stress in the longitudinal direction is insignificant, the transverse residual stress on the inside surface decreases with increasing yield strength.
2. The welding process may introduce residual stress in weldment of the higher magnitude than the yield strength of the base material.
3. The load-deflection response is sensitive to the effect of residual stresses. The existence of residual stress can decrease the stiffness of the sigma beam and the strain hardening can increase the peak load of sigma beams.
4. It can be found that the cold work in corner regions can improve the load resistance capability of simply supported sigma beam while the residual stress in flat portions reduces the failure load of each specimen.

References

[1] Tan, Z., Li, W.B. and Persson, B. (1994) "On analysis and measurement of residual stresses in the bending of sheet metals", *Int. J. Mech. Sci.*, 36 (5), 483-491.

[2] Zhang, Z.T. and Hu, S.J. (1998) "Stress and residual stress distributions in plane strain bending", *International Journal of Mechanical Sciences*, 40 (6), 533-543.

[3] Quach, W.M., Teng, J.G. and Chung, K.F. (2004) "Residual stresses in steel sheets due to coiling and uncoiling: a closed-form analytical solution", *Journal of Engineering Structures*, 26, 1249-1259.

[4] Weng, C. C. and White, R. N. (1990) "Residual Stresses in Cold-bent Thick Steel Plates", *Journal of Structural Engineering*, 116(1), 24-39.

[5] Quach, W.M., Teng, J.G. and Chung, K.F. (2006) "Finite element predictions of residual stresses in press-braked thin-walled steel sections", *Engineering Structures*, Vol. 28, 1609-1619.

[6] Teng, T.L., Chang, P.H. and Tseng, W.C. (2003) "Effect of welding sequences on residual stresses", *Computers and Structures*, 81, 273–286.

[7] Yaghi, A., Hyde, T.H., Becker, A.A., Sun, W. and Williams, J.A. (2006) "Residual stress simulation in thin and thick-walled stainless steel pipe welds including

pipe diameter effects", *International Journal of Pressure Vessels and Piping*, 83, 864–874.

[8] Jameel, A.N., Nabeel, K. and Osama, F. (2010) "Residual stress distribution for a single pass weld in pipe", *Journal of Engineering, Volume 16*.

[9] Kong, F., Ma, J. and Kovacevic, R. (2011) "Numerical and experimental study of thermally induced residual stress in the hybrid laser–GMA welding process", *Journal of Materials Processing Technology*, 211, 1102-1111.

[10] Heinze, C., Schwenk, C. and Rethmeier, M. (2012) "Numerical calculation of residual stress development of multi-pass gas metal arc welding", *Journal of Constructional Steel Research*, 72, 12–19.

[11] Huber, A.W. (1956) "The influence of residual stress on the instability of columns", Fritz Laboratory reports of Lehigh University, 1496.

[12] Huber, A.W. and Ketter, R.L. (1958) "The influence of residual stress on the carrying capacity of eccentrically loaded columns", Fritz Laboratory reports of Lehigh University, 1503.

[13] Beedle, L.S., and Tall, L. (1960) "Basic Column Strength", *Journal of the Structural division*, ASCE, Vol. 86.

[14] Weng, C.C. (1991) "Effects of residual stress on cold formed steel column strength", *Journal of Structural Engineering*, vol. 117, 1622-1640.

[15] Quach, W.M., Teng, J.G. and Chung, K.F. (2010) "Effect of the manufacturing process on the behaviour of press-braked thin-walled steel columns", *Engineering Structures*, 32: 3501–3515.

[16] Gao, T. and Moen, C.D. (2010) "The cold work of forming effect in steel structural members", *Stability and Ductility of Steel Structures*, Rio, Brazil.

[17] Yu, W.W. (2003) "Cold-formed steel design", 3rd edition, Missouri, US.

[18] Weng, C.C. and Pekoz, T. (1990) "Residual stresses in cold formed steel members", *J. Struct. Div.*, ASCE, 116(6), 1611-1625.

[19] Deng, D. (2009) "FEM prediction of welding residual stress and distortion in carbon steel considering phase transformation effects", *Materials and Design*, Vol. 30: 359–366.

[20] Deng, D. and Murakawa, H. (2006) "Numerical simulation of temperature field and residual stress in multi-pass welds in stainless steel pipe and comparison with experimental measurements", *Computational Materials Science*, Vol. 37: 269–277.

[21] Brickstad, B. and Josefson, B. L. (1998) "A parametric study of residual stresses in multi-pass butt-welded stainless steel pipes", *International Journal of Pressure Vessels and Piping*, 75, 1l-25.

[22] BSI (2001). Metallic materials-Tensile testing-Part 1: Method of test at ambient temperature, BS EN 10002-1:2001.

[23] Chakrabarty, J. (2006) "Theory of plasticity (3rd edition)", Published by Elsevier Butterworth-Heinemann, Oxford, UK.